Line shape of the plasma resonance in simple metals*

P. C. Gibbons, S. E. Schnatterly, J. J. Ritsko,† and J. R. Fields‡
Department of Physics, Joseph Henry Laboratories, Princeton University, Princeton, New Jersey 08540
(Received 2 September 1975)

Energy spectra of plasmons with wave vectors from 0 to k_F are reported in aluminum, sodium, and lithium. The dispersion of the peak position and of the width are given for aluminum and sodium, and it is shown that free-electron theory with simple damping and exchange corrections can be made to reproduce the shape of the plasma resonance at all wave vectors studied.

INTRODUCTION

Adequate theoretical understanding of the degenerate electron gas is a long-standing problem, still unsolved at metallic densities. Inelastic electron scattering,[1] differential in energy loss and momentum transfer, measures directly the Fourier transform $S(q, \omega)$ of the space- and time-dependent electron pair correlation function, the structure factor for the electrons in the sample. Stated another way, inelastic electron scattering allows experimental determination of the frequency- and wave-vector-dependent dielectric screening function $\epsilon(q, \omega)$, which describes the response of the electrons in the sample to an applied charge-density fluctuation. In this paper we report studies of simple metals by measurements of the shape of the plasma resonance energy spectrum as a function of wave vector, up to the Fermi wave vector.

BACKGROUND

Previous measurements of electron energy-loss spectra versus momentum transfer have been reported by Swanson and Powell[2]; Ninham, Powell, and Swanson[3]; Zacharias[4]; Kloos[5]; Kunz[6]; Silcox and co-workers[7]; and Petri and Otto.[8] Powell and Swanson analyzed their data on aluminum for the width and energy of the plasmon as a function of its wave vector, out to about 1.5 $Å^{-1}$ where the peak disappeared into the multiple scattering background. Zacharias measured the plasmon width and energy in aluminum as a function of wave vector out to about 2 $Å^{-1}$. Kloos measured the energy and width versus wave vector with high resolution in wave vector. Petri and Otto and Silcox and co-workers report measurements similar to Zacharias's. Using x-ray Compton scattering, Eisenberger and co-workers have measured the large wave-vector behavior of plasmons in single crystals of Al, Be, Li, and graphite.[9,10] They show a peak or shoulder with small or negative dispersion, at wave vectors greater than the Fermi wave vector, which may be characteristic of the electron gas rather than any particular material.[11]

Our results are sufficiently accurate and free of multiple scattering effects to allow comparison between experimental and theoretical plasmon line shapes for momenta up to k_F.

APPARATUS AND SAMPLES

Plasmon measurements were made with an inelastic electron scattering facility recently built at Princeton.[1] The primary beam energy of this device is 300 keV. In all these experiments the resolution wave between 80 and 150 meV in energy loss and between 0.08 and 0.15 $Å^{-1}$ in momentum transfer. Energy-loss spectra were measured for fixed momentum transfer at a number of different momenta.

Most of the data were taken by pulse-counting techniques, allowing multiscanning and signal averaging to reduce effects of slow systems drifts during data acquisition. The noise in the data is not noticeably greater than that due to counting statistics; typically on the order of 1% or less. Errors due to beam intensity drifts are on the order of 0.1% or less in most of the data.

Thin, self-supporting samples were needed for these transmission experiments. We made polycrystalline aluminum samples by coating microscope slides with a water soluble wax, Victawet,[12] polishing the coating, and evaporating aluminum onto the coated surface. The films were floated off the slide onto the surface of a tray of water, where they could be picked up with a copper frame. Once attached to the frame they stuck fast and could withstand gentle handling. We made measurements on three aluminum samples, approximately 1100, 800, and 500 Å thick. Surface oxide and contamination was tolerated because the limiting oxide thickness at room temperature is approximately 40 Å, which should not cause too great a correction at these sample thickness. Surface excitations were detected, but they did not interfere with our measurements. Sodium and lithium were evaporated in the sample chamber onto thin Formvar[12] substrates. These attenuated the beam by 10% or less and have no sharp features in their spectra,

while the alkali samples attenuated the beam by more than 50%. The inelastic scattering from the Formvar was too small to be seen in any of the data reported here. The alkali samples were evaporated and the measurements made in an O-ring sealed vacuum of about 10^{-7} Torr. Measurements began the instant the evaporation was completed, and the first measurements could be repeated to monitor sample contamination. In time chemically shifted core excitations would appear and the structure below the plasmon—the surface plasmon and other features—would change. None of the data reported in this study was affected by aging in the 8–12 h in which it was taken.

For sample thickness such that a particular inelastic scattering event is improbable but elastic scattering is strong, which is a typical situation, the counting rate for the inelastic process is

$$N = N_0 e^{-\alpha l} k l ,$$

where N_0 is the primary beam particle current and l is the sample thickness. The scattering probabilities per unit length are α for elastic scattering out of the beam and k for the particular inelastic process being studied. This counting rate is maximum for a sample thickness $l = 1/\alpha$ such that the transmitted unscattered beam current is $1/e$ of the incident current. An electron that is scattered elastically and once inelastically will contribute to the background in any measurement. For example, elastic scattering with momentum transfer q followed by forward scattering creating a zero wave-vector plasmon produces a peak at the zero wave-vector plasmon energy in spectra taken at higher wave vectors, as in Fig. 2. The relative strength of multiple scattering decreases with decreasing thickness.

In previous experiments as in this one, the condition above was approximately satisfied. Early experiments indicated that evidence of excitations of the conduction electrons vanished at approximately the cutoff wave vector. This was due to relatively large backgrounds caused by multiple inelastic scattering in thick samples. Recent experiments have seen spectra well beyond cutoff. In this experiment we measure spectral line shapes even in samples over 1000 Å thick. We can use such thick samples because of the dependence of the inelastic scattering probability k on primary energy and our very low "no beam" or dark detector signal of one count per second. k is approximately proportional to eV_0^{-1}, where eV_0 is the kinetic energy of the primary beam. Thus there is less multiple inelastic scattering in our experiment than in others, because of the higher beam energy.

THEORY

The differential scattering cross section per atom, per unit energy loss, per unit solid angle, for fast electrons transmitted through solid samples, is, in the Born approximation[13]

$$\frac{d^2\sigma}{d\Omega dE} = \frac{1}{N}\left(\frac{2}{q^2 a_0}\right)^2 \times \sum_f \left|\langle\psi_f|\sum_j e^{i\vec{q}\cdot\vec{r}_j}|\psi_0\rangle\right|^2 \delta(E_f - E_0 - E), \tag{1}$$

which can be rewritten

$$\frac{d^2\sigma}{d\Omega dE} \sim \frac{1}{q^2}\,\mathrm{Im}\left(\frac{-1}{\epsilon(\vec{q},\omega)}\right), \tag{2}$$

where ψ_f is a many-electron final state and ψ_0 is the initial state. The sum on j is over all electrons in the solid, and N is the number of atoms in the solid. E_f and E_0 are the final and initial energy of the sample. $E = \hbar\omega$ is the energy loss, $\hbar q$ is the momentum transfer, and a_0 is the first Bohr radius. $\epsilon(q,\omega)$ is the generalized longitudinal dielectric response function for the solid. For small momentum transfer ($q \approx \omega/c$), ϵ is equivalent to the optical dielectric constant. For fast electrons $\hbar q \cong P_0\theta$, where P_0 is the initial beam momentum and θ the scattering angle. Thus, for forward scattering, $\theta \approx 0$, an electron scattering experiment measures the optical dielectric constant.[14,15]

The usual starting point in discussing screening in an electron gas is Lindhard's longitudinal dielectric response function for a noninteracting electron gas[16,17]:

$$\epsilon(\vec{q},\omega) = 1 + \frac{3}{128\gamma^2 Z^3} \times \left\{4Z + [1-(U-Z)^2]\ln\frac{U-Z-1}{U-Z+1} - [1-(U+Z)^2\ln\frac{U+Z-1}{U+Z+1}\right\}, \tag{3}$$

$$Z = \left|\frac{\vec{q}}{2k_F}\right|, \quad U = \frac{\hbar\omega}{4ZE_F},$$

where γ is the ratio of the Fermi energy to the plasma energy, E_F is the Fermi energy, and k_F is the Fermi wave vector. Principle values are to be used for the logarithms in case of negative or complex arguments. At excitation energies such that $U \gg Z+1$, the function becomes simply[18]

$$\epsilon(\vec{q},\omega) = 1 - \frac{\omega_p^2}{\omega^2}, \quad h\omega \gg 4E_F\,\frac{q}{2k_F}\left(\frac{q}{2k_F}+1\right),$$

where ω_p is the plasma frequency. This predicts that all of the strength is in an infinitely sharp peak, at $\omega = \omega_p$, in the $q = 0$ energy-loss spectrum. Expanding the full expression in powers of γ gives the small q behavior of the spectra. The peak disperses and loses strength, and single-particle excitations appear at low energies.[14,17,19] Above the cutoff wave vector q_c, the single-particle spectrum overlaps the plasmon peak as shown in

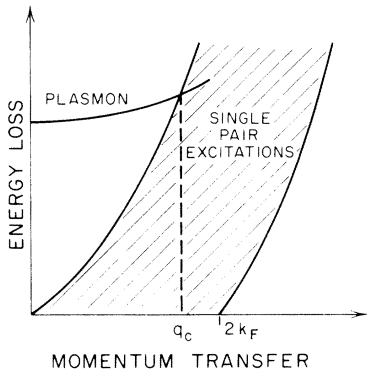

FIG. 1. Cutoff wave vector q_c for a plasmon, at or beyond which it can decay into a single pair excitation.

Fig. 1. For $q \gg q_c$, the Compton scattering limit, the plasmons will entirely disappear leaving only the single-particle spectrum. For $q \gtrsim q_c$ the plasmon is no longer a well-defined excitation, but manifests itself as an enhancement in the single-particle spectrum.

In this description of conduction electrons, there is no damping; each excited state is treated as long lived. The interaction between electrons is approximated by making each electron move in an average potential produced by all the rest, as in the Hartee approximation. Exchange and correlation effects are left out.

The first modification of the Lindhard dielectric function indicated by the data is damping. The plasmon has finite width at all wave vectors. Even for small wave vectors, the wings of the plasmon and single-particle peaks overlap, so that they are not strictly separable. Strictly speaking, there is no well defined cutoff wave vector. Modifying the Lindhard dielectric function as shown by Mermin[20] adds simple phenomenological damping in a collision time approximation. Sharp features are broadened to a width equal to the imaginary part of the energy.

Correlation and exchange can be included approximately by a simple local-field correction

$$\epsilon(\vec{q},\omega) - 1 \to \frac{\epsilon(\vec{q},\omega) - 1}{1 - G(\vec{q},\omega)[\epsilon(\vec{q},\omega) - 1]} \,. \tag{4}$$

If G is a complex number, its imaginary part produces damping, but not the same as Mermin's.[21] A preliminary estimate[22] of $G(q,\omega)$ indicates that at finite frequency its imaginary part is nonzero.

We have tried to fit our data with damping from Mermin's collision time mechanism only and with damping from both mechanisms. From a very simple point of view the collision time can be thought of as describing the electron-phonon interaction and interband transitions, and the complex exchange damping can be taken to describe additional effects, e.g. electron-electron collisions. In attempting to fit our line shapes with this model, we have taken $\mathrm{Im}(E) = \hbar\Gamma$, $\mathrm{Im}(G)$, and $\mathrm{Re}(G)$ to be frequency-independent functions of the wave vector [$\mathrm{Re}(E) = \hbar\omega$ is the energy loss]. To improve the precision of the model without adding new parameters, we include in the dielectric function the effect of the polarizability of the atomic cores,[23,24] $4\pi\chi_{\mathrm{core}}$. The resulting dielectric function is

$$\begin{aligned}
&\epsilon(\vec{q},\omega + i\Gamma) - 1 = N/D\,,\\
&N = (\omega + i\Gamma)[\epsilon_L(\vec{q},\omega + i\Gamma) - 1 + 4\pi\chi_{\mathrm{core}}]\,,\\
&D = \omega\{1 - G(\vec{q})[\epsilon_L(\vec{q},\omega + i\Gamma) - 1]\}\\
&\quad + i\Gamma\{1 - G(\vec{q})[\epsilon_L(\vec{q},0) - 1]\}\\
&\quad \times \frac{\epsilon_L(\vec{q},\omega + i\Gamma) - 1 + 4\pi\chi_{\mathrm{core}}}{\epsilon_L(\vec{q},0) - 1 + 4\pi\chi_{\mathrm{core}}}\,,
\end{aligned} \tag{5}$$

where $\epsilon_L(\vec{q},\omega + i\Gamma)$ is the Lindhard function, Eq. (3). The Fermi energy is chosen to be consistent with photoemission bandwidths,[25] band structure calculations,[26] and with soft x-ray emission bandwidths.[27] The plasma frequency is chosen to give the observed zero wave-vector plasmon energy. The values chosen for these are listed in Table I.

DATA AND ANALYSIS

Typical data for aluminum are shown in Figs. 2 and 3, for sodium in Fig. 4, and for lithium in Fig. 5 Figures 6 and 7 show the sample to sample reproducibility for our data in aluminum and lithium. The large width of the lithium plasmon at all wave vectors, probably due to a stronger crystal field, makes detailed curve fitting relatively unprofitable, so we concentrate on aluminum and sodium. The data show clearly many important multiple scattering features, found in all electron energy-loss data, which must be subtracted from the data before any analysis can be done. We shall discuss these features in our sodium data. Due to our high beam energy and thin samples these effects are small enough to be easily removed. At $q = 0$, in addition to the sharp plasmon peak near 7 eV, there are surface plasmons at lower

TABLE I. Parameters used in fitting plasmon line shapes in Na and Al.

	Na	Al
Fermi wave vector (Å^{-1})	0.92	1.75
Fermi energy (eV)	3.24	11.1
Plasma energy (eV)	6.05	15.4
Ion core-polarizability contribution to the dielectric function	0.14	0.05

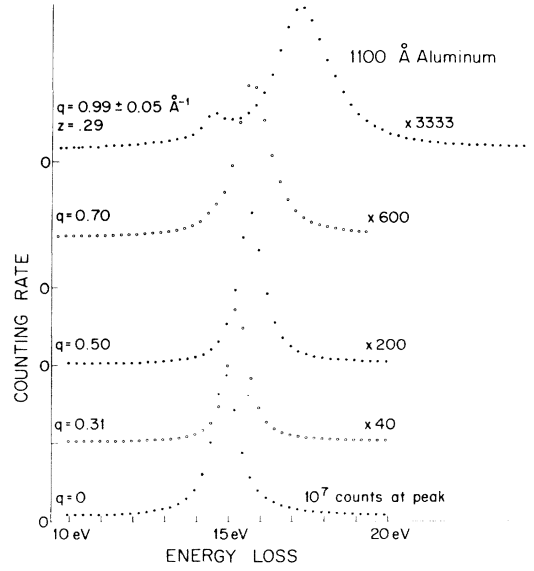

FIG. 2. Electron-energy-loss spectra of aluminum at various momentum transfers. Statistical uncertainties are smaller than the plotted points.

energy. These are clearly separated from the bulk plasmon and, as momentum transfer increases, lose strength more rapidly than bulk excitations. We ignore these surface excitations in our analysis.

As momentum transfer $\hbar q$ increases, the plasmon disperses to higher energy and broadens. Beginning at $q = 0.68$ Å^{-1} and clearly in the data at $q = 0.85$ Å^{-1}, there is a peak at the zero wave-vector plasmon energy with approximately the zero wave-vector width. This is due to double

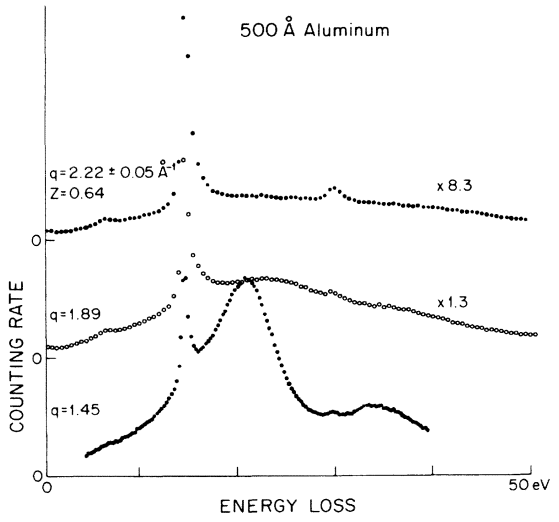

FIG. 3. Electron-energy-loss spectra of aluminum at large momentum transfers. The scatter in the points is due to statistical fluctuations.

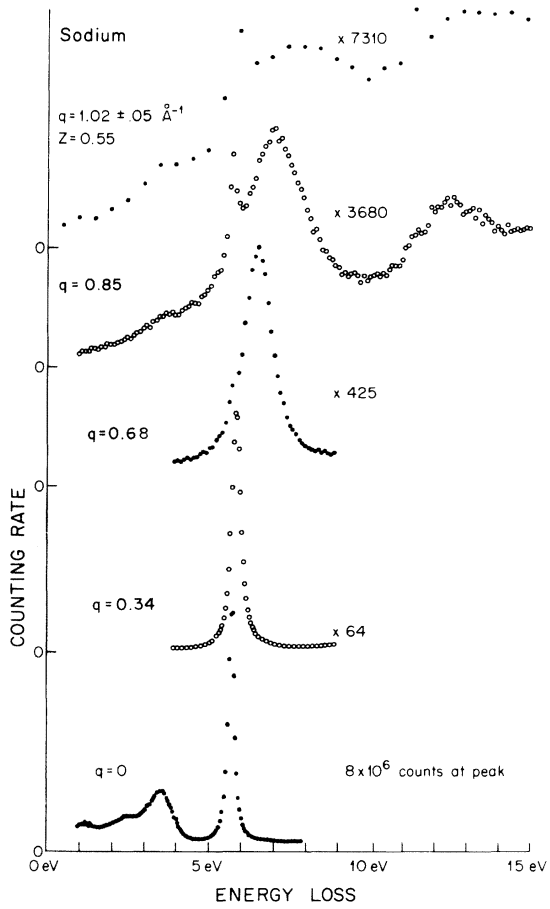

FIG. 4. Electron-energy-loss spectra of sodium at various momentum transfers. In the large-q curves, the scatter in the points is due to statistical fluctuations.

scattering involving a lattice scattering event and a plasmon scattering event with wave vector q'. Direct measurements show that the strength of the lattice scattering (at zero energy loss, with the 0.1 eV resolution used here) is independent of wave vector, so the resemblance to the zero wave-vector plasmon spectrum is entirely due to the $(q')^{-2}$ weighting from the inelastic cross section. These double scattering features involving the lattice and a bulk plasmon can easily be removed from the data because they are highly localized in energy. Similar features involving a surface plasmon are less localized and more difficult to subtract, but are also considerably weaker.

Triple scattering involving the lattice can be seen in the highest wave-vector spectrum from sodium, at twice the zero wave-vector bulk plasmon frequency. Triple scattering involving the lattice and a bulk and a surface plasmon is too weak, even at the highest wave vector, to significantly modify the shape of the observed spectrum.

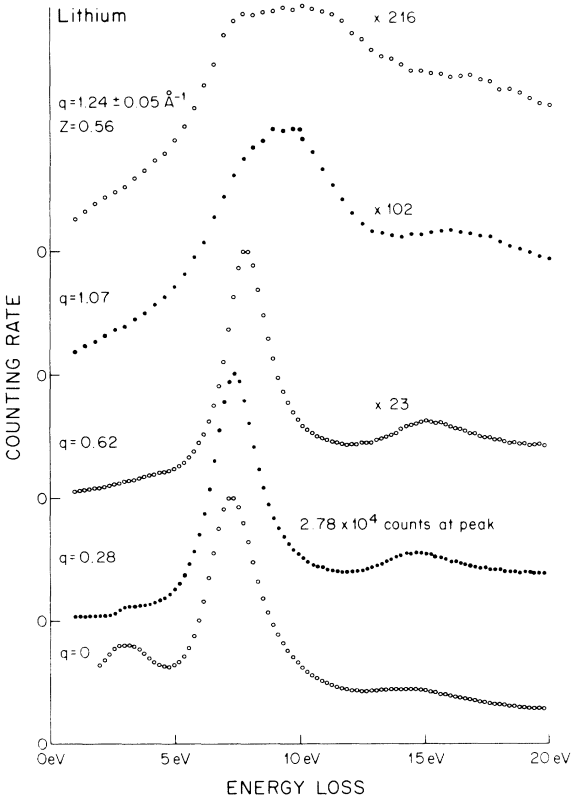

FIG. 5. Electron-energy-loss spectra of lithium at various momentum transfers. In the large-q curves, the scatter in the points is due to statistical fluctuations.

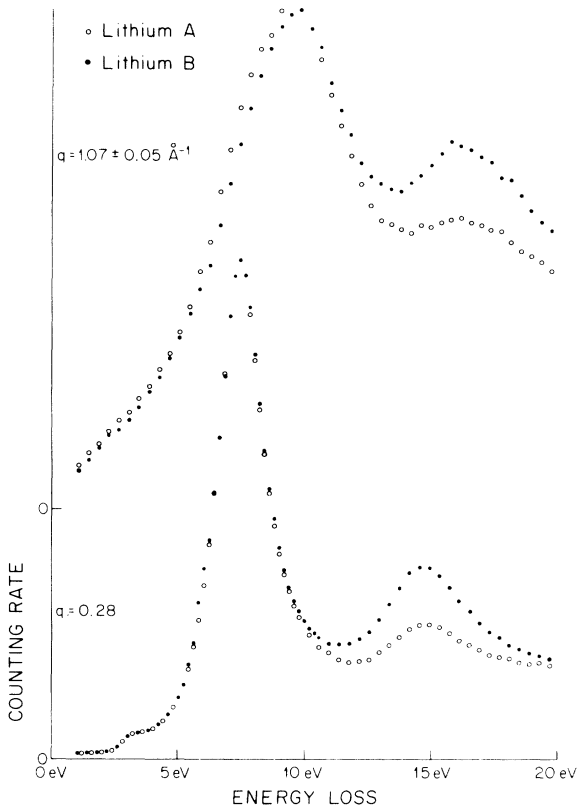

FIG. 7. Spectra at 0.28 and 1.07 Å^{-1} momentum transfer for two different lithium samples (A and B) are compared. Despite noticeable differences in the multiple scattering background above the plasmon peaks, there is little difference between samples at plasmon peaks.

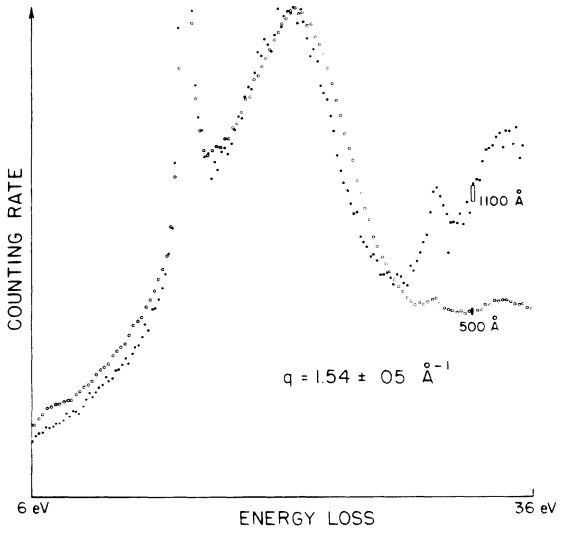

FIG. 6. Spectra at 1.51 Å^{-1} momentum transfer for two different aluminum samples, with counting statistics shown by boxes at the right. Despite the large change in multiple scattering background above the plasmon peak, there is little difference between the samples at the peak.

Multiple inelastic scattering is the most difficult effect to subtract in data taken at large wave vectors. The peaks at 13–14 eV in the 0.85- and 1.02 Å^{-1} spectra are due to double plasmon scattering events. These, and presumably higher multiples as well, give a background which increases with energy in the vicinity of the plasmon. Clearly, at 1.02 Å^{-1} there is a dispersed plasmon at about 8 eV, but its shape cannot be seen without a reliable background subtraction.

Observation of many spectra from samples of various thicknesses, mainly aluminum, has made it clear that the shape of the double plasmon peak at wave vector q_0, which must be represented by a three-dimensional convolution of single scattering spectra (one energy loss, two momentum transfer directions), can be qualitatively reproduced by a one dimensional convolution in energy loss of the single plasmon spectrum for wave vector $q_0/2$. It is the q^{-2} weighting in the cross section that makes this the dominant contribution. For energies lower than the two-plasmon peak energy, the one-dimensional convolution has an

energy dependence close to AE^3, where E is the energy loss, for all wave vectors q_0.

A background AE^3 has therefore been subtracted from the data before fitting with the modified Lindhard-Mermin spectrum. The constant A and the other fitting parameters are determined by a weighted least-squares alogrithm. The procedure yields two useful results. First, a background subtraction is performed, by the same method at all wave vectors, in as unbiased a manner as is possible. The subtracted data can be analyzed for position and width of the plasmon. Second, a model of the data using only a few parameters is obtained by fitting the data with the modified Lindhard-Mermin function, and those parameters have a very simple q dependence.

RESULTS

Figure 8 shows the dispersion of the plasmon in sodium, plotted using variables natural for the small wave-vector limit of the Lindhard dielectric function. Two simple measures of peak position are used and both give similar results. Figure 8 also shows the width of the plasmon in the sodium at various wave vectors. The width increases linearly with q^2 at all wave vectors, but the rate of that variation increases sharply at about the cutoff wave vector q_c. This is consistent with the simple picture of the Landau damping

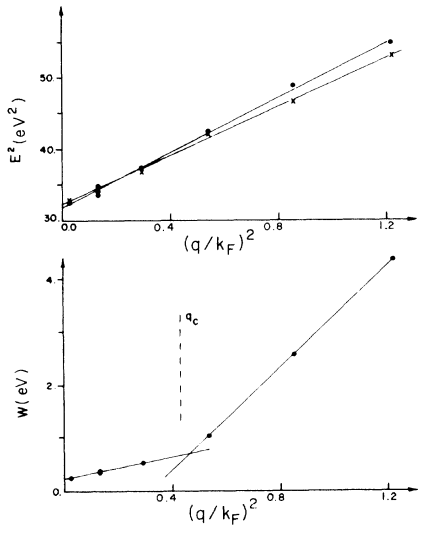

FIG. 8. Above: Dispersion of the sodium plasmon. q is the plasmon wave vector and k_F the Fermi wave vector 0.92 Å^{-1}. E is the energy of the plasmon, circles from the peak and crosses from the average of the half height energies. The dispersion of the peak is $E_{peak}{}^2 = 19.4(q/k_F)^2\ \text{eV}^2 + [E(z=0)]^2$. Below: Full width at half-height W of the sodium plasmon. The cutoff, marked by the verticle dashed line, is calculated with an exchange correction (Ref. 28).

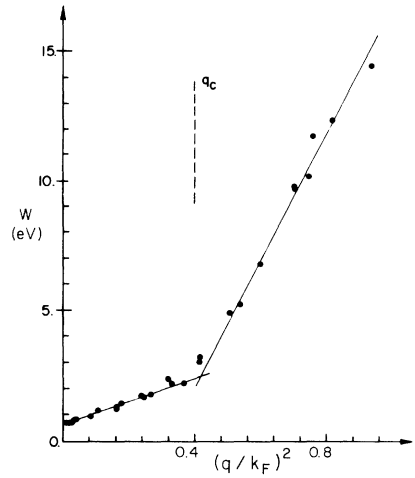

FIG. 9. Full width at half-height W of the aluminum plasmon. q is the plasmon wave vector and k_F the Fermi wave vector 1.75 Å^{-1}. The cutoff shown by the vertical dashed line is calculated with an exchange correction (Ref. 28).

turning on at q_c, opening up a new decay channel.

Figure 9 shows the width of the aluminum plasmon at various wave vectors. The behavior is the same as in the sodium data. In each case the measure of width used is the energy difference between half-peak intensity points. The wave vectors at which the curves change slope are consistent, in each material, with the cutoff wave vector calculated including an exchange correction[28] to the dispersion. Without the exchange correction the calculated cutoff wave vectors are larger than the values at which the width curves change slope.

Figure 10 shows the energy of the aluminum plasmon as a function of wave vector q. The position of the peak (measured with a constant energy resolution of ~0.1 eV) is a simple linear function of q^2, while the average of the two half-peak energies disperses more slowly for $q > q_c$ (again, calculated with an exchange correction). This is easily understood. In aluminum the shape of the plasmon spectrum is symmetric at small wave vectors but becomes increasingly asymmetric above q_c. The high-q spectra show more scattering strength at an energy $\hbar\Delta\omega$ below the plasmon peak than at $\hbar\Delta\omega$ above. The resolution with which spectra are measured must be considerably finer than the widths of these asymmetric plasmons to locate the peak energy correctly. Measurements obtained by varying the energy resolution of the apparatus to keep up counting rates at large wave vectors must be corrected for these asymmetry errors even if the peak is used as the measure of position.[5]

We show the dispersion of the plasmon in lithium

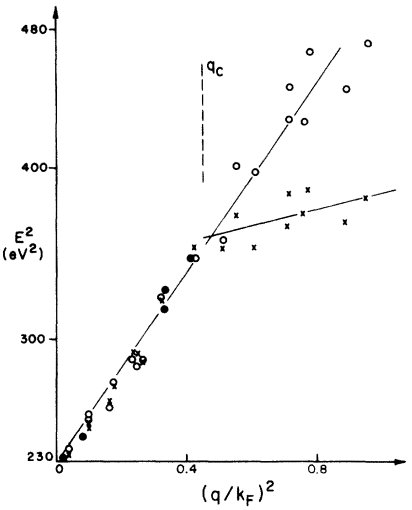

FIG. 10. Dispersion of the aluminum plasmon. q is the plasmon wave vector and k_F the Fermi wave vector 1.75 Å^{-1}. E is the plasmon energy, circles from the peak and crosses from the average of the half-height energies. The dispersion of the peak is $E_{peak}^2 = 290(q/k_F)^2$ eV^2 + $[E(z=0)]^2$. The vertical dashed line marks the cutoff wave vector, calculation with an exchange correction (Ref. 28).

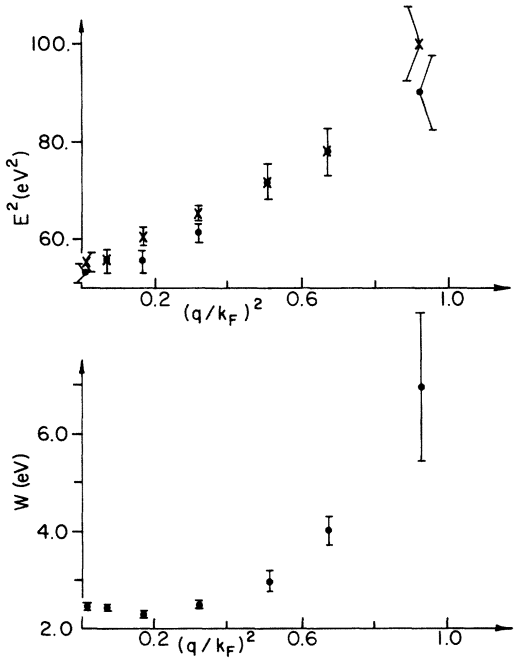

FIG. 11. Above: Dispersion of the lithium plasmon. q is the plasmon wave vector and k_F the Fermi wave vector, 1.12 Å^{-1}. E is the plasmon energy, circles from the peak and crosses from the average of the half height energies. The dispersion of the peak is approximately $E_{peak}^2 = 43(q/k_F)^2$ eV^2 + $[E(q=0)]^2$. Below: Full width at half-height W of the lithium plasmon. The error brackets include estimated uncertainties in the background.

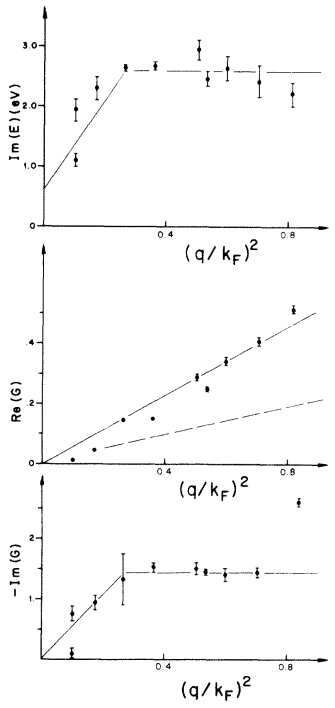

FIG. 12. Fitted values of Im(E), Re(G), and Im(G) with standard deviations computed by the least-squares-fitting program, for aluminum. Only spectra including background over a broad range about the plasma energy are shown. These were used to develop the simple model of the q dependence shown by the solid lines. The dashed line for Re(G) is from Vashishta and Singwi (Ref. 28).

in Fig. 11. The background in this data was estimated, since the fitting function was not used. The variation of width with q^2 is clearly more complicated here than in Na or Al.

Because of the method by which the inelastic multiple scattering background was subtracted, it is not simple to estimate uncertainties in the results discussed above. The scatter of the aluminum results, from samples of different thicknesses and ages, is probably the best indication of the precision of our conclusions. Figures 6 and 7 demonstrate the reliability, in our data, of any consistently applied background subtraction at all but the highest wave vectors measured.

The modified Lindhard-Mermin fitting function, while not perfect, does give reasonable agreement at all wave vectors measured. The parameters which give the best fits show considerable scatter, but indicate very simple wave vector dependences. Figures 12 and 13 show the results for aluminum and sodium. As can be seen all parameters are piecewise linear in q^2. Simple analytic expressions for the straight lines drawn are given in Table II.

Spectra calculated with parameters obtained from Table II fit the data more poorly in some cases, better in others. On the whole, they do

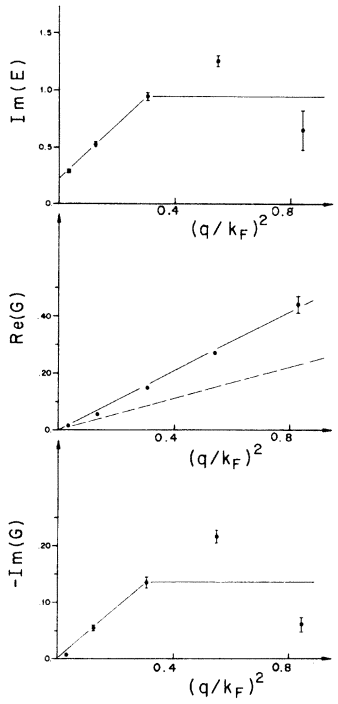

FIG. 13. Fitted values of Im(E), Re(G), and Im(G) with standard deviations computed by the least-squares-fitting program, for sodium. The solid lines are the simple model of the q dependence, developed from the points shown, with the constraint that it be similar to the aluminum model. The dashed line for Re(G) is from Vashishta and Singwi (Ref. 28).

about as well as the "best" fits. The uncertainties in the aluminum parameters are derived from the scatter of the "best" fits about the straight lines drawn in Fig. 13, so that roughly 70% of the fits fall within the uncertainty limits.

A simpler fitting model may be used. Requiring $\mathrm{Im}[G(q)] = 0$ reduces the dielectric function used to the Lindhard-Mermin function modified only by core polarizability and static exchange corrections. The agreement with the data is, however, significantly poorer. The elements of the fitting exercise are displayed in Figs. 14 and 15, which show aluminum data at wave vectors 0.90 and 1.47 Å^{-1} and calculations made with the model discussed above. In the fits using a real exchange correction, the imaginary energy is smaller than it is with the complex exchange correction, and the exchange parameter G assumes essentially the same value as Re(G) in the fits with complex exchange corrections.

At 0.90 Å^{-1} there is little difference between the best fits obtained with real and with complex exchange parameters G. The simple model of Fig. 13 fails to reproduce the position as well as the best fits. At 1.47 Å^{-1}, the reason for introducing

TABLE II. Simple parametrization of the fitting variables used in the modified Lindhard-Mermin dielectric function. Z is $q/2k_F$.

Sodium:

$$\mathrm{Im(E)} = \begin{cases} 0.22 + 9.6Z^2 \text{ eV}, & Z^2 < 0.076 \\ 0.95 \text{ eV}, & Z^2 \geq 0.076 \end{cases}$$

$$\mathrm{Re(G)} = 2.02Z^2$$

$$\mathrm{Im(G)} = \begin{cases} -1.79Z^2, & Z^2 < 0.076 \\ -0.136, & Z^2 \geq 0.076 \end{cases}$$

Aluminum:

$$\mathrm{Im(E)} = \begin{cases} 0.53 + 30.9Z^2 \pm 0.2 \text{ eV}, & Z^2 < 0.067 \\ 2.60 \pm 0.2 \text{ eV}, & Z^2 \geq 0.067 \end{cases}$$

$$\mathrm{Re(G)} = 2.5Z^2 \pm 0.05$$

$$\mathrm{Im(G)} = \begin{cases} -2.12Z^2 \pm 0.2, & Z^2 < 0.067 \\ -0.142 \pm 0.2, & Z^2 \geq 0.067 \end{cases}$$

a complex exchange correction becomes evident. The calculation with a real exchange parameter cannot correctly reproduce both the position and width of the peak because its asymmetry is too great. The calculation with a complex exchange correction has a much more appropriate shape. Its most noticeable failure is that its peak strength

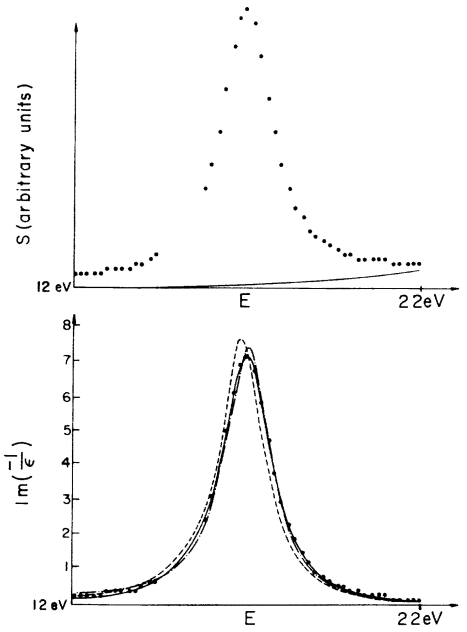

FIG. 14. Measured and calculated spectra at a wave vector of 0.90 Å^{-1} in aluminum. Top: The measured spectrum S and the part due to background, determined by the fitting procedure described in the text. Bottom: The data after background subtraction (points) and the calculated loss functions. Solid line, the best fit with a complex exchange coefficient. Dashed line, using parameters from Table II. Dot-dashed line, best fit with a real exchange coefficient.

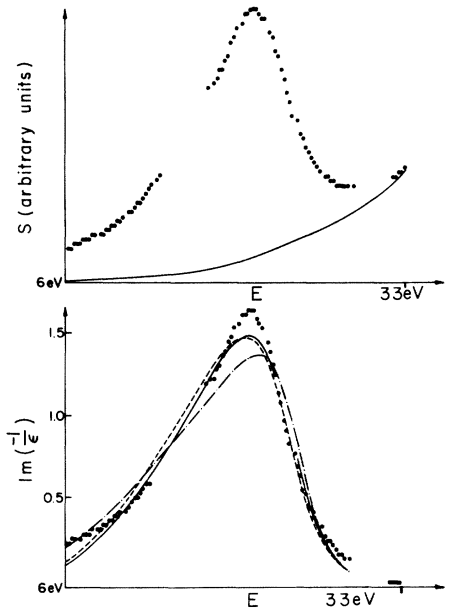

FIG. 15. Measured and calculated spectra at a wave vector of 1.47 Å^{-1} in aluminum. Top: The measured spectrum S and the part due to background, determined by the fitting procedure described in the text. Bottom: The data after background subtraction (points) and the calculated loss functions. Solid line, the best fit with a complex exchange coefficient. Dashed line, using parameters from Table II. Dot-dashed line, best fit with a real exchange coefficient.

to wing strength ratio is not quite high enough to match the data. The model of Fig. 13 is essentially the same as the best fit at this wave vector. The features pointed out here are found in all the data taken in aluminum and sodium, and the agreement between the data and the calculation here is typical.

The oscillator-strength sum rule

$$\int_0^\infty \mathrm{Im}[-\epsilon(q,\omega)^{-1}]\,\omega\,d\omega = \tfrac{1}{2}\pi\omega_p^2, \tag{6}$$

where ω_p is the plasma frequency, was used to test the data. For wave vectors from 0.9 to 1.6 Å^{-1} in aluminum the sum remained constant to within 5% of its average value. The sum was consistent with the known plasma frequency, which proves our background subtraction is correct in the total area it accounts for in the data.

COMPARISON WITH OTHER EXPERIMENTS AND THEORY

The data of Kloos[5] for aluminum show a small wave-vector (q) deviation from the expected quadratic dispersion, and in lithium he saw a deviation from the simple quadratic dependence of the width on q at small q. The q resolution in the present experiments is not as good as that of Kloos.[5] In aluminum the anomaly Kloos observed occurs for q smaller than our resolution. In lithium we agree with Kloos, finding a minimum in the width of the plasmon at about 0.5 Å^{-1}. This is probably due to scattering of the plasmon at grain boundaries, as suggested by Krishan and Ritchie.[29]

More recently Petri and Otto[8] have reported a deviation from quadratic dispersion in aluminum for $0 \le q \le 0.6$ Å^{-1}. Data from the present experiment show no such effect.

The present measurements, made in polycrystalline samples with wave vectors up to the Fermi wave vector, show no narrow small dispersion peak as seen by Eisenberger *et al.*[9,10] nor any identifiable precursor of that peak, although a slowing of the dispersion of the center of gravity of the entire conduction-electron spectrum is expected, and seen in aluminum. It is due to the asymmetry of the spectrum, with greater strength at low energies, which is caused by single-particle excitations, and it increases with wave vector.

Zacharias[4] and Petri and Otto[8] both show the dispersion of the plasmon in aluminum at small wave vectors q,

$$\omega = \omega_p + \alpha(\hbar/m)\,q^2. \tag{7}$$

Petri and Otto find $\alpha = 0.401$, Zacharias's graph is consistent with $\alpha = 0.40$, and we find $\alpha = 0.42$ consistent with the other values when the scatter in the data is taken into account. In sodium we find $\alpha = 0.24$.

Zacharias[4] fits his dispersion curve for the aluminum plasmon with an exchange correction like ours, but constrained to be real, in a Lindhard-Mermin dielectric function with wave-vector-independent damping. Using the small wave-vector form $G(q) = \gamma q^2$, which seems from our data to be valid over the entire range from zero to the Fermi wave vector, Zacharias found $\gamma = 0.63$, exactly the same as our result and 2.4 times larger then the value given by Vashishta and Singwi.[28] In sodium we find $\gamma = 0.51$, which is larger than the value of Vashishta and Singwi by a factor of 1.8. We have observed that increasing the damping decreases the dispersion coefficient α in the Lindhard-Mermin model for the spectra, if the peak energy is taken to be the plasmon energy. The simple relation between α and γ which obtains when there is no damping must fail in all real metals, as it does for the sodium and aluminum data reported here and the aluminum data of Zacharias.

CONCLUSION

The wave-vector dependence of the plasmon characteristic energy-loss function has been studied in Li, Na, and Al. Analysis of the few Na and many Al measurements shows that, when due care is taken to treat multiple scattering problems adequately and when data are taken with

sufficiently fine energy resolution, the wave vector (q) dependence of the width and peak energy of the plasmon are simple. The behavior of the plasmon width at the cutoff wave vector is qualitatively understood, although the small q plasmon width has never been fully explained.[30] The dispersion of the peak behaves as predicted by Lindhard's dielectric function out to $q \cong k_F$, the Fermi wave vector.

A simple model for the shape of the spectrum at all wave vectors up to k_F is given, based on a modified Lindhard function. It is hoped that the sucess of this model may stimulate additional interest in the quest for a theoretically adequate model dielectric function consistent with all the available electron gas excitation data.

---

*Work supported by NSF Grant No. GH-34646.

†Present address: Xerox Webster Research Center, 800 Phillips Rd. W-114, Webster, N.Y. 14580.

‡Present address: Dept. of Biophysics, The Johns Hopkins University, Baltimore, Md. 21218.

[1]P. C. Gibbons, J. J. Ritsko, and S. E. Schnatterly Rev. Sci. Instrum. (to be published).

[2]N. Swanson and C. J. Powell, Phys. Rev. 145, 195 (1966).

[3]B. W. Ninham, C. J. Powell, and N. Swanson, Phys. Rev. 145, 209 (1966).

[4]P. Zacharias, Z. Phys. 256, 92 (1972); J. Phys. C 7, L26 (1974); and J. Phys. F 5, 645 (1975).

[5]T. Kloos, Z. Phys. 265, 225 (1973); and thesis (Universitat Hamburg, 1973) (unpublished).

[6]C. Kunz, Z. Phys. 196, 311 (1966); 167, 53 (1962).

[7]J. Silcox, Bull. Am. Phys. Soc. 20, 282 (1975); and P. E. Batson, C. H. Chen, and J. Silcox, *ibid.* 22, 410 (1975).

[8]E. Petri and A. Otto, Phys. Rev. Lett. 34, 1283 (1975).

[9]P. Eisenberger, P. M. Platzman, and K. C. Pandey, Phys. Rev. Lett. 31, 311 (1973); and P. Eisenberger, P. M. Platzman, and P. Schmidt, *ibid.* 34, 18 (1975).

[10]P. M. Platzman and P. Eisenberger (private communication).

[11]G. Hukhopadhyay, R. K. Kalia, and K. S. Singwi, Phys. Rev. Lett. 34, 950 (1975).

[12]Victawet: Victawet 35B, Stauffer Chemical Co., Industrial Div., 380 Madison Ave., New York, N. Y. 10017. Formvar: a vinyl-acetal resin varnish used to insulate magnet wire (The Electric AutoLite Co., Wire and Cable Div.).

[13]D. Pines, *Elementary Excitations in Solids* (Benjamin, New York, 1964).

[14]H. Raether, Springer Tracts Mod. Phys. 38, 85 (1965).

[15]J. Daniels, C. V. Festenberg, H. Raether, and K. Zeppenfeld, Springer Tracts Mod. Phys. 54, 77 (1970).

[16]J. Lindhard, K. Dan. Vidensk. Selsk. Mat.-Fys. Medd. 28, No. 8 (1954).

[17]A. J. Glick and R. A. Ferrell, Ann. Phys. (N.Y.) 11, 359 (1960).

[18]J. M. Ziman, *Principles of the Theory of Solids*, 2nd ed. (Cambridge U.P., London, 1972).

[19]P. M. Platzman and P. A. Wolff, *Waves and Interactions in Solids State Plasmas*, Solid State Phys. Suppl. 13 (Academic, New York, 1973).

[20]N. D. Mermin, Phys. Rev. B 1, 2362 (1970).

[21]G. D. Mahan (private communication).

[22]P. Vashishta (private communication).

[23]S. L. Adler, Phys. Rev. 126, 413 (1962).

[24]J. H. Van Vleck, *Electric and Magnetic Susceptibilities* (Oxford, U.P., Oxford, 1932).

[25]Y. Baer and C. Busch, Phys. Rev. Lett. 30, 280 (1973).

[26]F. Ham, Phys. Rev. 128, 82 (1962); 128, 2524 (1962); W. F. Rudge, *ibid.* 181, 1024 (1969); L. Dagens and F. Perrot, Phys. Rev. B 8, 1281 (1973).

[27]E. T. Arakawa and M. W. Williams, Phys. Rev. B8, 4075 (1973); W. F. Hanson and E. T. Arakawa, Z. Phys. 251, 271 (1972); and G. A. Rooke, In *Soft X-Ray Band Spectra and the Electronic Structure of Metals and Materials*, edited by D. J. Fabian (Academic, New York, 1968).

[28]P. Vashishta and K. S. Singwi, Phys. Rev. B 6, 875 (1972).

[29]V. Krishan and R. H. Ritchie, Phys. Rev. Lett. 24, 1117 (1970).

[30]D. F. Dubois and M. G. Kivelson, Phys. Rev. 186, 409 (1969), and references given there.